Large-eddy simulation of supersonic planar jets impinging on a flat plate at an angle of 60 to 90 degrees

Romain Gojon*, Christophe Bogey† and Olivier Marsden‡

Laboratoire de Mécanique des Fluides et d'Acoustique

UMR CNRS 5506, Ecole Centrale de Lyon

69134 Ecully, France

Six planar supersonic jets are computed by compressible large-eddy simulations (LES) using low-dissipation schemes. At the exit of a nozzle of height h, they are ideally expanded and have an exit velocity u_e, yielding a Mach number of $\mathcal{M}_e = 1.28$, and a Reynolds number of $Re_h = u_e h/\nu = 5 \times 10^4$. Four jets impinging on a flat plate at distances L from the nozzle lips ranging from $3.94h$ up to $9.1h$, with an angle θ between the jet direction and the plate of 90 degrees, are first considered. Two other jets with $L = 5.5h$ and $\theta = 60$ and $\theta = 75$ degrees are also examined. In this way, the effects of both the nozzle-to-plate distance and the angle of impact on the flow and acoustic fields of the jet are studied. Mean velocity flows and snapshots of density, pressure and vorticity are shown. The pressure fields are also described by computing sound pressure levels and using Fourier decomposition. Several tones are obtained in certain cases and their corresponding Strouhal numbers and symmetric or antisymmetric natures are in agreement with experimental data and theoretical models. They are due to an aeroacoustic feedback mechanism occurring between the nozzle lips and the flat plate. This mechanism generates an hydrodynamic-acoustic standing wave revealed by using Fourier decomposition.

I. Introduction

Jets impinging on a flat plate have been studied experimentally by many authors over the past sixty years. In some cases, very intense tones have been observed in the acoustic field. In his pioneering work, in 1953, Powell[1] suggested that they are due to a feedback mechanism between hydrodynamic instabilities propagating downstream from the nozzle lip to the plate and acoustic waves propagating upstream from the plate to the nozzle lips.

Round subsonic jets impinging on a flat plate normally for an exit Mach number ranging from 0.3 up to 0.9 have been studied notably by Ho and Nosseir[2] and Nosseir and Ho[3] in the eighties. The near pressure field was described using microphones and a simplified model predicting the frequencies of the feedback mechanism based on cross-correlations between the microphones was proposed. Round supersonic jets impinging on a flat plate normally have also been investigated experimentally by Henderson and Powell,[4] Krothapalli *et al.*[5] and Henderson *et al.*[6] and more recently by Risbord and Soria[7] and Buchmann *et al.*[8] using high-speed optical measurements. In some cases, a feedback mechanism similar to those in subsonic jets was found. This mechanism appears very often when the jet is ideally expanded but only for some nozzle-to-plate distances when the jet is imperfectly expanded. Henderson *et al.*[6] suggested that in the latter case, the feedback establishes only when a Mach disk forms upstream from the plate.

Planar jets impinging on a flat plate normally also produce intense tone frequencies. However, compared to round jets, tones are visible at lower flow velocities, as noted by Arthurs and Ziada.[9] Planar supersonic jets impinging on a flat plate normally has been studied by Norum[10] and Tam and Norum[11] in the nineties. These authors obtained, for certain jets, acoustic spectra with two emerging tone frequencies. The lower

*PhD, romain.gojon@ec-lyon.fr.

†CNRS Research Scientist, AIAA Senior Member & Associate Fellow, christophe.bogey@ec-lyon.fr.

‡olivier.marsden@ec-lyon.fr.

tone frequency is due to a varicose (symmetric) mode of the jet, and the upper tone frequency is due to a sinuous (antisymmetric) mode. Similar tone frequencies have been found in a 2-D simulation by Hourigan *et al.*[12] In order to understand the varicose or sinuous behaviour of the jet, Tam and Norum[11] proposed that the upstream propagating waves of the feedback mechanism are neutral acoustic wave modes of the jet. Thus, both the wave number k and the angular frequency ω of these modes are real. They found an allowable frequency range for each upstream propagating neutral acoustic wave mode of the jet flow using a vortex sheet jet model and noted that the two emerging tones observed in the experiment of Norum[10] fall into the first symmetric and the first antisymmetric allowable bands given by the model. Later, several tone frequencies for supersonic rectangular impinging jets have also been detected experimentally by Thurow *et al.*[13] using a real-time flow visualization technique. A coupling between the organization of the hydrodynamic structures in the shear layers of the jets and the degree of resonance of the feedback mechanism was pointed out.

For non-normal impingement angle, the intensity of the feedback mechanism decreases because of the loss of symmetry. Indeed, Norum[10] conducted an experiment for a supersonic ideally expanded planar jet impinging on a inclined flat plate and noted that the amplitude of the strongest impingement tone decreases when the angle of impact deviates from 90 degrees. Besides, to understand the lift-off phase of a space launcher, Nonomura *et al.*[14,15] performed the 2-D simulation of a jet impinging on a inclined plate and the LES of a 3-D supersonic ideally expanded round jet impinging on a inclined plate. They obtained three types of waves in the acoustic field, namely the Mach waves generated in the jet shear layers, the Mach waves from the shear layer of the supersonic flow on the inclined flat plate, and the waves coming from the impingement region. These three types of waves were analysed by Tsutsumi *et al.*[16] using a snapshot proper orthogonal decomposition with Fourier transformation. Moreover, the transient regime of supersonic jets was investigated by Dargaud *et al.*[17] by conducting the simulation of the ignition overpressure wave generated by horizontal rocket motors interacting with the ground.

In the present work, LES of six planar jets are carried out in order to investigate the feedback mechanism between the nozzle lips and the flat plate. In particular, their spectral and hydrodynamic properties are studied and compared to empirical and theoretical models. The paper is organized as follows. The main characteristics of the jets and the simulations are presented in section II. Mean fields, snapshots and acoustical results are shown in section III and compared with experimental data. The feedback mechanism is then studied in section IV by applying Fourier decomposition to the pressure field. Finally, concluding remarks are given in section V.

II. Parameters

II.A. Jets parameters

Large-eddy simulations are performed for four jets impinging normally on a flat plate for nozzle-to-plate distances L/h of 3.94, 5.5, 8.27, and 9.1. For the nozzle-to-plate distance $L/h = 5.5$, two other simulations are carried out for the angles of impact $\theta = 60$ and 75 degrees between the jet axis and the flat plate. The different cases are presented in table 1. They are referred to as JetL3, JetL5, JetL8, JetL9, JetL5-60d and JetL5-75d, respectively. The jets originate from a planar nozzle of height h, and width $l = 3.25h$ in the spanwise direction. The lip thickness is $e = 0.5h$, and periodic conditions are imposed in the spanwise direction, allowing planar jets to be investigated. The ejection conditions of the jets and the nozzle-to-plate distances are similar to the parameters in the experimental study of Thurow *et al.*[13] Thus, the jets are ideally expanded, and have a Mach number of $\mathcal{M}_e = 1.28$. Their Reynolds number is $Re_h = u_e h/\nu = 5 \times 10^4$. A Blasius mean velocity profile is imposed at the nozzle exit with a boundary-layer thickness of $\delta_{BL} = 0.075h$.

II.B. Numerical parameters

In the four cases where the angle between the jet axis and the flat plate is 90 degrees, the unsteady compressible Navier-Stokes equations are solved on a Cartesian mesh for which x, y and z denote the longitudinal, lateral and spanwise directions, respectively. An explicit six-stage Runge-Kutta algorithm is used for time integration, and low-dispersion eleven-point explicit finite differences are used for spatial derivation.[18,19] At the end of each time step, a relaxation filtering is applied to the flow conservative variables in order to remove grid-to-grid oscillations and to dissipate subgrid-scale turbulent energy. The radiation conditions of Tam and Dong[20] are implemented at the inflow and lateral boundaries of the computational domain. A sponge zone combining grid stretching and Laplacian filtering is also employed to damp the turbulent fluctuations

	$\mathcal{M}_e$	Re_h	L/h	θ
JetL3	1.28	5×10^4	3.94	90 degrees
JetL5	1.28	5×10^4	5.5	90 degrees
JetL8	1.28	5×10^4	8.27	90 degrees
JetL9	1.28	5×10^4	9.1	90 degrees
JetL5-60d	1.28	5×10^4	5.5	60 degrees
JetL5-75d	1.28	5×10^4	5.5	75 degrees

Table 1. Jet parameters: Mach number $\mathcal{M}_e$, Reynolds number $Re_h = u_e h/\nu$, nozzle-to-plate distance L, and angle θ between the jet direction and the flat plate.

before they reach the lateral boundaries. Adiabatic conditions are imposed to the nozzle wall and the flat plate. Examples of 3-D jets simulated using the present solver can be found in Bogey and Bailly[21,22] for transitional round jets at a Mach number $\mathcal{M}_e = 0.9$ and for self-similar turbulent round jets at a Mach number $\mathcal{M}_e = 0.9$. A shock-capturing filtering is applied in order to avoid Gibbs oscillations near shocks. It consists in applying a conservative second-order filter optimised in Fourier space at a magnitude determined each time step using a shock sensor.[23] This method was successfully used by de Cacqueray *et al.*[24] for the LES of an overexpanded jet at a fully developed Mach number $\mathcal{M}_j = 3.3$. Finally, vortical disturbances not correlated in the spanwise direction[25] are added in the boundary layer in the nozzle near $x = -0.5h$ and $y = 0.45h$ in order to generate velocity fluctuations at the nozzle exit. The strength α of the forcing is settled to 0.02 to obtain turbulent intensities between 5% and 10% at the nozzle exit, as it will be reported in the next section. This value is similar to those used used in Bogey *et al.*[25]

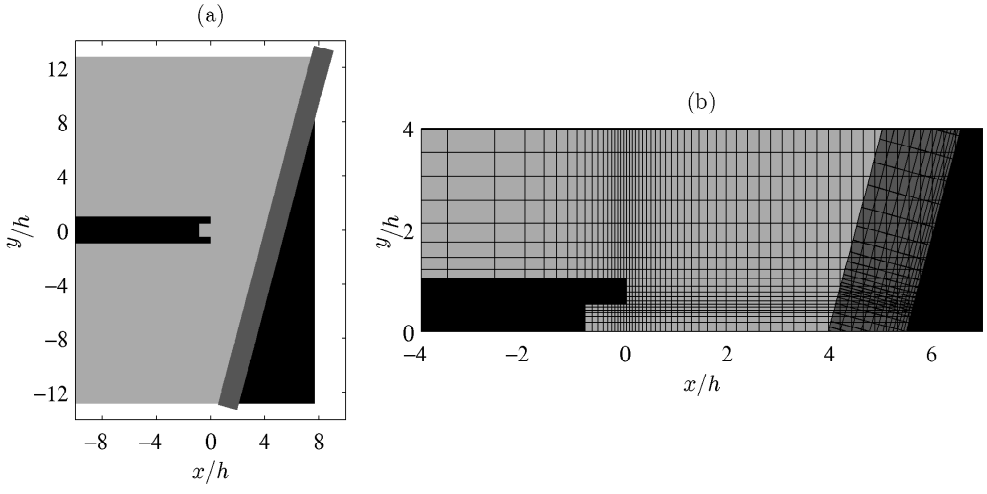

Figure 1. Representation of the two Cartesian meshes used in the case JetL5-15d: (a) meshes sketch of the two meshes, with the primary grid in light grey, the secondary grid in dark grey and the nozzle and flat plate in black and (b) representation of the grids, every fifteen points is shown.

In the two cases where the angle between the jet axis and the flat plate is 60 and 75 degrees, two Cartesian meshes are used as presented in figure 1. The mesh containing the nozzle is referred to as the primary grid and the mesh close to the flat plate as the secondary grid. The two meshes are identical in the spanwise direction z, allowing the flow variables to be transferred from one grid to another using a 2-D interpolation in the (x, y) plane. For the interpolation, a high-order Lagrangian 2-D interpolation based on a 10-point stencil is used in each direction. The numerical methods used are identical to those of the four LES with $\theta = 90$ degrees.

The simulations are carried out using an OpenMP-based in-house solver, and a total of $200,000$ iterations are computed in each case for the steady state. The simulation time is thus equal to $500h/u_e$. The Cartesian meshes contain between 184 and 263 million points for the primary grids and between 38 and 46 million points for the secondary grids, as noted in table 2 and in table 3. For JetL3, JetL5, JetL8 and JetL9, the variations of the axial and lateral mesh spacings are represented in figure 2. The minimal axial mesh spacing, near the nozzle lip and the flat plate, is equal to $\Delta x = 0.00375h$ and the maximal axial mesh

	n_x	n_y	n_z	number of points
JetL3	799	1051	219	184×10^6
JetL5	903	1051	219	208×10^6
JetL8	1087	1051	219	250×10^6
JetL9	1142	1051	219	263×10^6
JetL5-60d	1196	801	219	210×10^6
JetL5-75d	966	901	219	191×10^6

Table 2. Parameters of the primary grids containing the jets.

	n_x	n_y	n_z	number of points
JetL5-60d	181	1151	219	46×10^6
JetL5-75d	181	961	219	38×10^6

Table 3. Parameters of the secondary grids close to the plate, used for the cases with inclined plates.

spacing, between the nozzle and the plate, is equal to $\Delta x = 0.015h$. The lateral mesh spacings are equal to $\Delta y = 0.00375h$ at $y = \pm h/2$ and to $\Delta y = 0.03h$ for $2.5h \leq y \leq 8h$. The spanwise spacings are equal to $\Delta z = 0.015h$. This discretization allows acoustic waves with Strouhal numbers up to $St_h = fh/u_e = 5.6$ to be well propagated, where f is the frequency. The grids are stretched at rates lower than 1% outside the sponge zones in order to preserve numerical accuracy. For JetL5-60d and JetL5-75d, the primary meshes are designed with a minimal axial mesh spacing near the nozzle lip equal to $\Delta x = 0.00375h$ and a maximal axial mesh spacing downstream from the nozzle equal to $\Delta x = 0.015h$. The lateral mesh spacings are similar to those for JetL3. The secondary meshes have a minimal axial mesh spacing equal to $\Delta x = 0.00375h$ close to the plate and a maximal axial mesh spacing equal to $\Delta x = 0.015h$ upstream from the plate. The lateral mesh spacings are similar to those for jetL3 and are designed to minimize the difference in mesh size between the two grid as illustrated in figure 1(b).

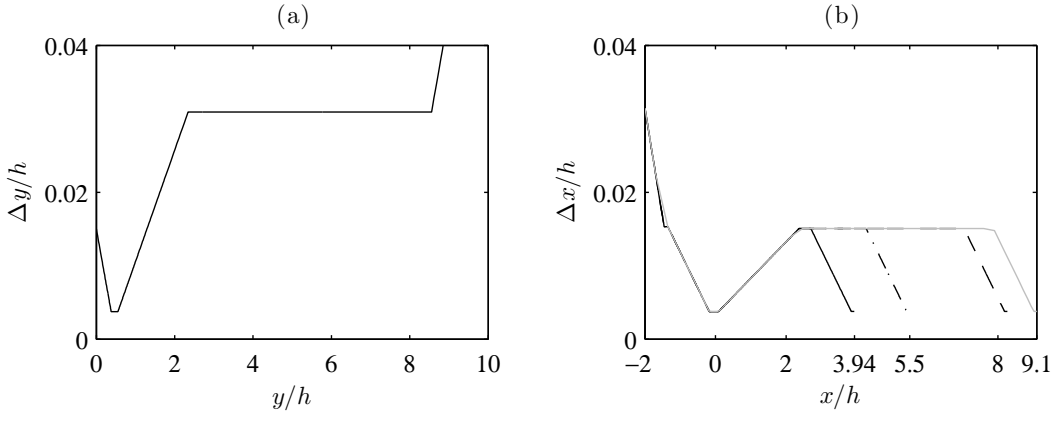

Figure 2. Representation of (a) the lateral mesh spacings, and (b) the axial mesh spacings: —— JetL3, —·— JetL5, — — — JetL8, and —— JetL9.

III. Results

III.A. Mean flow fields

Mean velocity fields obtained in the (x, y) plane are shown in figure 3 for JetL3, JetL5, JetL8 and JetL9 and in figure 4 for JetL5, JetL5-75d and JetL5-60d. As expected, very little variations (around 4% of the jet exit velocity) of the mean axial velocity are noticed near the axis, indicating that the jets are almost ideally expanded. In all cases, a stagnation point is visible on the flat plate at $y = 0$ and boundary layers appear on the plate on each side of the jet. For JetL3, JetL5, JetL8 and JetL9, the maximum velocity and the thickness of the boundary layer on the flat plate at $y = 2h$ are given in table 4. The maximum velocity of

the boundary layer decreases and the boundary-layer thickness increases with the nozzle-to-plate distance.

For JetL5, JetL5-75d and JetL5-60d, the developments of the top and bottom boundary layers are different. The maximum velocity and the thickness of the boundary layer at $y = \pm 2$ are given in table 5. When the angle of impact is not normal, the top boundary layer is thicker and its maximum velocity increases. Moreover, shock cells are visible in the upper boundary layer for JetL5-60d in figure 4(c). On the contrary, the maximum velocity and the thickness of the bottom boundary layer decrease when the angle of impact deviates from 90 degrees.

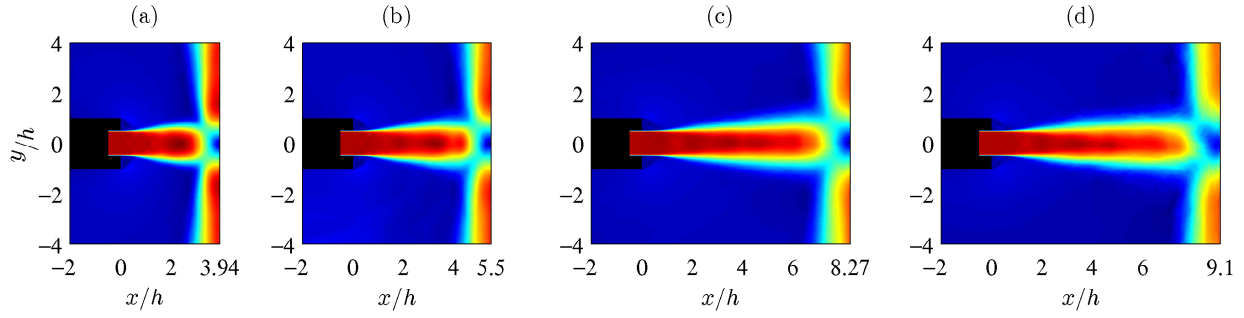

Figure 3. Mean velocity field in the (x, y) plane for (a) JetL3, (b) JetL5, (c) JetL8 and (d) JetL9. The colour scale ranges from 0 to 400 m.s^{-1}. The nozzle is represented in black.

	U_{max} $(m.s^{-1})$	δ_{99}/h
JetL3	361	1.25
JetL5	349	1.34
JetL8	316	1.56
JetL9	291	1.67

Table 4. Maximum velocity and thickness of the boundary layer on the flat plate at $y = 2h$.

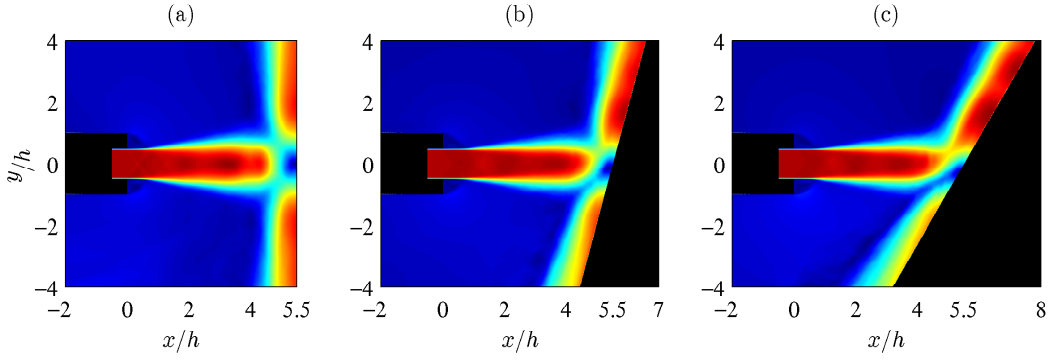

Figure 4. Mean velocity field in the (x, y) plane for (a) JetL5, (b) JetL5-75d and (c) JetL5-60d. The colour scale ranges from 0 to 400 m.s^{-1}. The nozzle and the flat plate are represented in black.

III.B. Flow snapshots

Snapshots of the vorticity norm obtained for JetL3, JetL5, JetL8 and JetL9 in the planes (x, y) and (x, z) along the lipline, are presented in figure 5. For JetL3, in figure 5(a), the two mixing layers exhibit large-scale structures, of typical size $0.5h$, in the (x, y) plane, which do not seem to be organized symmetrically with respect to the jet axis. In the spanwise direction, both small and large structures can be seen, namely tubes of vorticity along the entire spanwise extent and small vortical structures of typical size $0.05h$. Besides, the spanwise correlation of the vortical structures appears strong, near the nozzle but also close to the flat plate. For jetL5, JetL8 and JetL9, as the nozzle-to-plate distance increases, the asymmetric organisation of the large-scale structures in the two shear layers is still visible but its spanwise correlation seems to decrease in

	$y = 2h$		$y = -2h$	
	U_{max} $(m.s^{-1})$	δ_{99}/h	U_{max} $(m.s^{-1})$	δ_{99}/h
JetL5	349	1.34	349	1.34
JetL5-75d	372	1.36	328	1.22
JetL5-60d	374	1.62	291	1.23

Table 5. Maximum velocity and thickness of the boundary layer on the flat plate at $y = \pm 2h$.

the downstream direction. These observations are in agreement with the experimental results provided by Thurow *et al.*[13] for a rectangular supersonic jet impinging on a flat plate normally. Very large organized structures in the shear layers and an asymmetric pattern were indeed noted by the authors using real-time flow visualisation techniques.

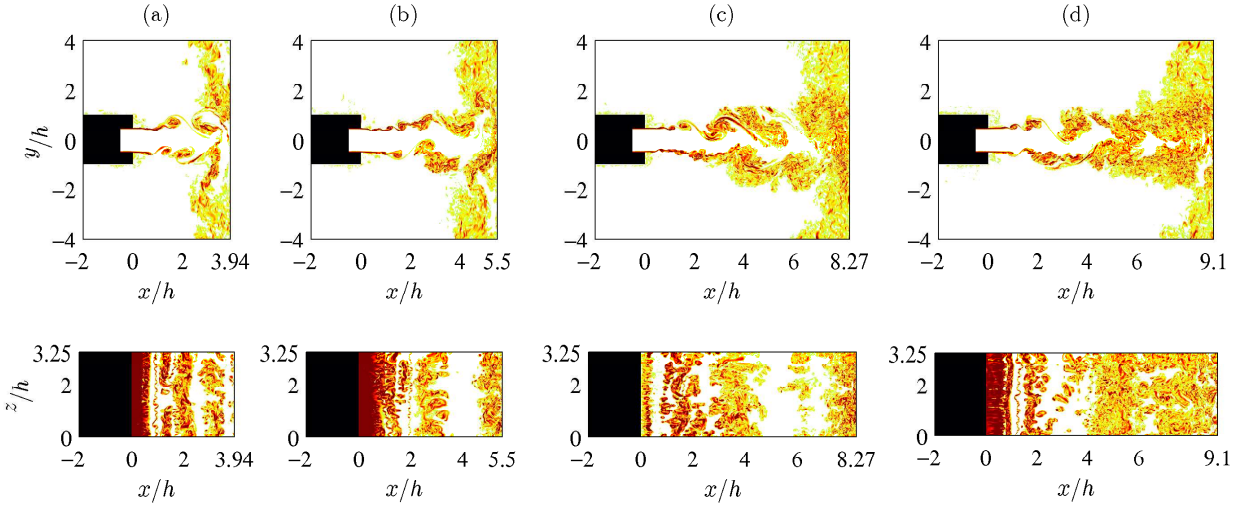

Figure 5. Snapshots in the planes (x, y) and (x, z) along the bottom lipline of the vorticity norm $|\omega|$ for (a) JetL3, (b) JetL5, (c) JetL8 and (d) JetL9. The colour scale ranges up to the level of $10u_e/h$. The nozzle is represented in black.

Snapshots of the vorticity norm obtained for JetL5, JetL5-75d and JetL5-60d in the planes (x, y) are presented in figure 6. The asymmetric organisation of the large-scale structures in the two shear layers, visible for the case JetL5 in figure 6(a), is less apparent as the angle of impact deviates from 90 degrees. Indeed, the pattern may still be noticed in figure 6(b) for JetL5-75d but can not for JetL5-60d in figure 6(c). Moreover, for JetL5-60d, the shear layers seem not to interact between each other.

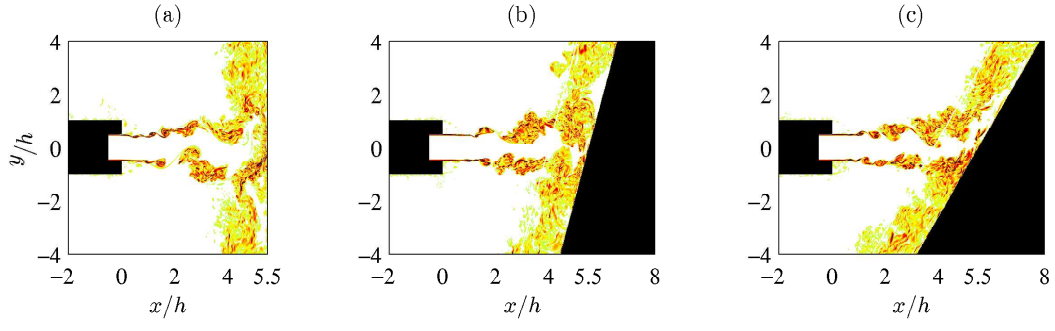

Figure 6. Snapshots in the (x, y) plane of the vorticity norm $|\omega|$ for (a) JetL5, (b) JetL5-75d and (c) JetL5-60d. The colour scale ranges up to the level of $10u_e/h$. The nozzle and the plate are represented in black.

In order to visualize the flow and acoustic fields of the jets, snapshots in the (x, y) plane of the density and the fluctuating pressure are provided in figure 7 for the four cases where the angle between the jet axis and the flat plate is 90 degrees and in figure 8 for the cases JetL5, JetL5-75d and JetL5-60d. Isolated

snapshots need to be considered with some cautions but they can provide qualitative results. For all cases, large-scale structures in the shear layers of the jet and sound waves are both observed. In figure 7, the sound waves seem to come from the region of impact of the jet and to have a higher amplitude for JetL3 and JetL5 than for JetL8 and JetL9. In figure 8, sound waves also appear to be generated from the region of impact, with amplitudes decreasing significantly as the angle of impact deviates from 90 degrees.

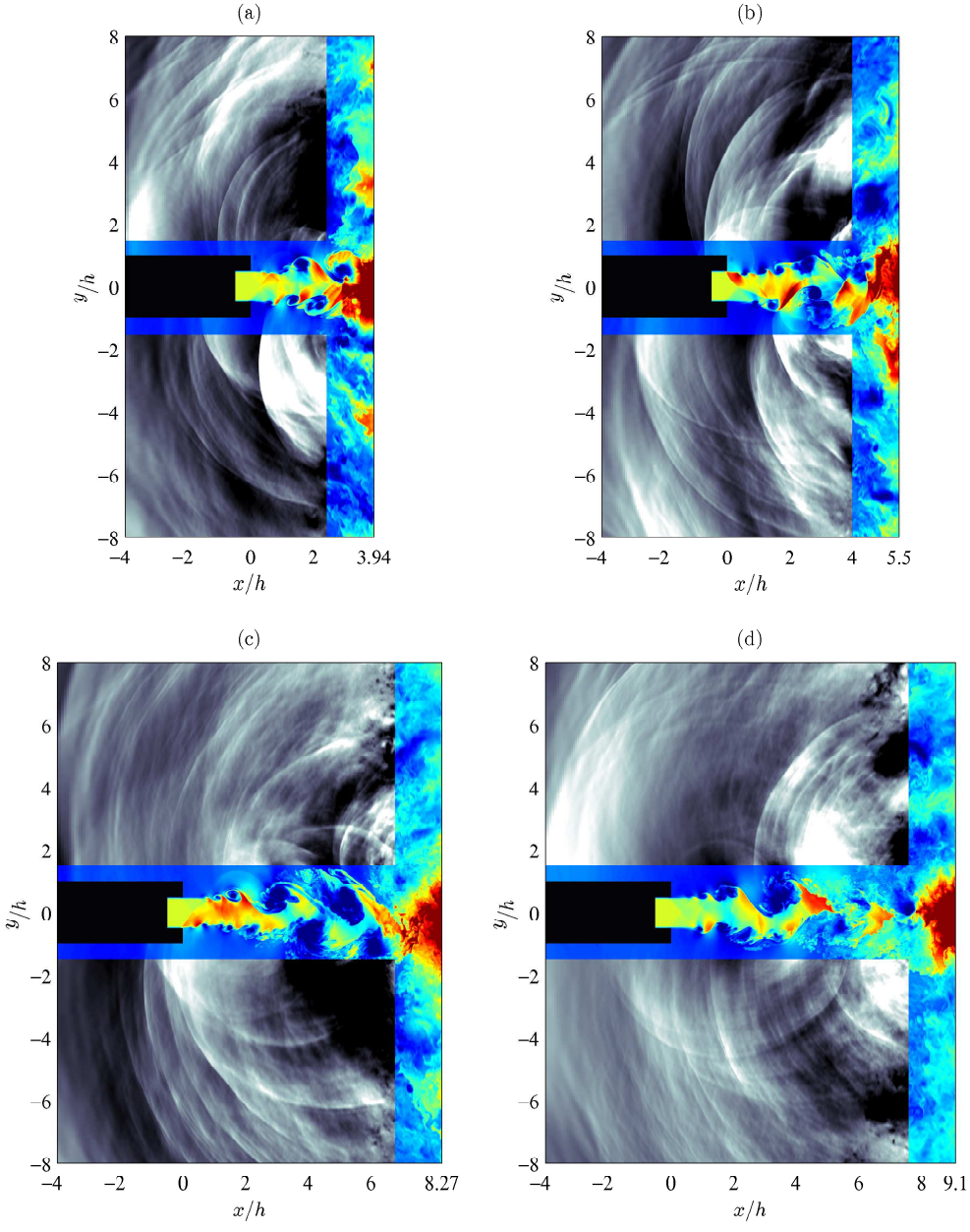

Figure 7. Snapshots in the (x, y) plane of the density in the jet axis and close to the flat plate and of the pressure fluctuations for (a) JetL3, (b) JetL5, (c) JetL8 and (d) JetL9. The colour scale ranges from 1 to 2 kg.m^{-3} for the density and from −7500 to 7500 Pa for the fluctuating pressure. The nozzle and the flat plate are represented in black.

Finally, there seems to be a correlation between the degree of organization of structures in the shear layers, noted in figures 5 and 6, and the amplitude of sound waves, observed figures 7 and 8. A similar trend was found experimentally by Thurow *et al.*[13]

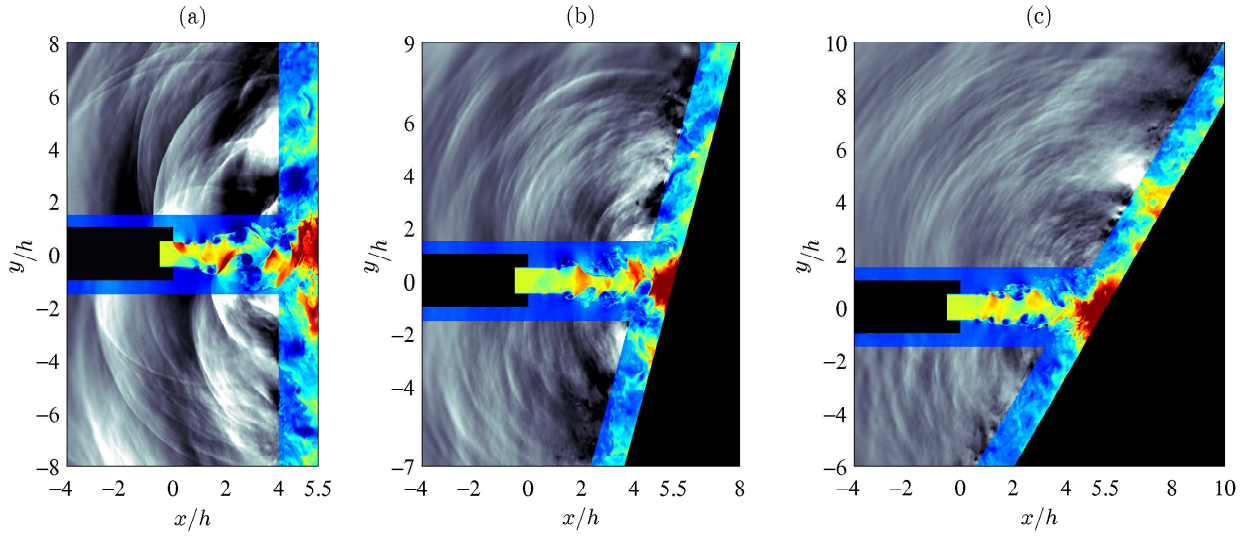

Figure 8. Snapshots in the (x, y) plane of the density in the jet axis and close to the flat plate and of the pressure fluctuations for (a) JetL5, (b) JetL5-75d and (c) JetL5-60d. The colour scale ranges from 1 to 2 kg.m^{-3} for the density and from −7500 to 7500 Pa for the fluctuating pressure. The nozzle is represented in black.

III.C. velocity fluctuations

The variations between the nozzle lips and the flat plate of the peak rms values of axial and transverse velocity fluctuations u' and v' obtained for JetL3, JetL5, JetL8 and JetL9 are shown in figure 9. For JetL3 and JetL5, the maxima of the peak rms values of axial velocity are found in figure 9(a) around $x = 0.5h$, and are equal to 31.8% and 32.7% of the jet exit velocity, respectively. For JetL8 and JetL9, the maxima of the peak rms values of axial velocity are located farther downstream, around $x = 0.75h$, and are equal to 26.6% and 27.3% of the jet exit velocity, respectively. For the four cases, other high peak rms values of axial velocity are also reached just before the plate. They decrease with the nozzle-to-plate distance, as they are equal to 28.5%, 27.3%, 24.4% and 24% of the jet exit velocity for JetL3, JetL5, JetL8 and JetL9. For the peak rms transverse velocity values in figure 9(b), it can be noted that higher values are observed for JetL3 and JetL5 than for JetL8 and JetL9. The nominal values, reached at $x = 1.7h$ in all cases, are around 21% of the jet exit velocity for JetL3 and JetL5, but 17.5% for JetL8 and JetL9.

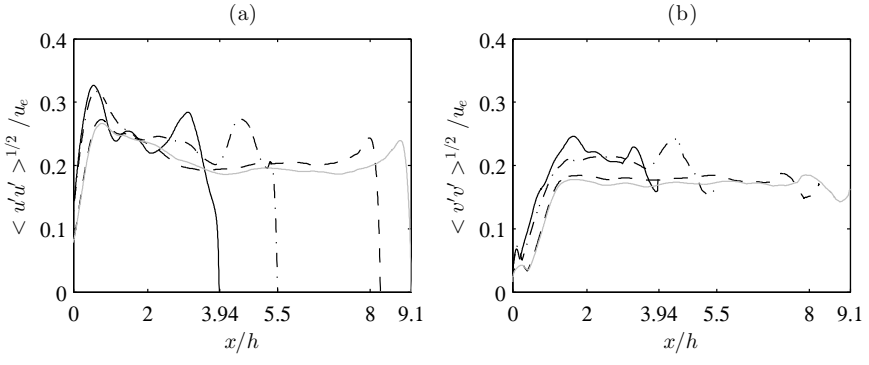

Figure 9. Variations of peak rms values of velocity fluctuations (a) u' and (b) v' for —— JetL3, —·— JetL5, — — — JetL8, and —— JetL9.

III.D. Convection velocity

The evolution of the large-scale structures in the shear layers and more precisely their convection velocity are of primary concern to understand the feedback mechanism between the nozzle and the flat plate. For two pressure-matched parallel streams with equal specific heats, the convection Mach number $\mathcal{M}_c$ was defined

by Papamoschou and Roshko[26] as

$$\mathcal{M}_c = \frac{u_1 - u_2}{a_1 + a_2} = \frac{u_1 - u_c}{a_1} = \frac{u_c - u_2}{a_2} \tag{1}$$

where u_1 and u_2 are the high-speed and low-speed free stream velocities, a_1 and a_2 are the speeds of sound, and u_c is the theoretical isentropic convection velocity. For the present planar jets, u_1 is the jet velocity at the nozzle exit u_e, u_2 is the velocity outside of the jet, hence $u_2 = 0$, a_1 is the speed of sound inside the jet $a_e = \sqrt{\gamma r T_e}$ and a_2 is the speed of sound outside of the jet $a_0 = \sqrt{\gamma r T_{amb}}$ where T_e and T_{amb} are the jet and the ambient temperatures. Thus, the convective velocity of the planar jet can be approximated by

$$u_c = \frac{u_e}{a_e/a_0 + 1} \tag{2}$$

For the present jets, a convection velocity of $u_c/u_e = 0.57$ is thus obtained. The convection velocity u_c of turbulent structures along the lipline $y = -h/2$ was also calculated from the cross-correlations of axial velocity fluctuations u'. In practice, for a reference point, cross correlations with twenty regularly-spaced neighbours are computed and the time lag between the reference point and its neighbours is fitted by a straight line. The derivative of the line gives then the local convective velocity. Results are shown in figure 10(a) for JetL3, JetL5, JetL8 and JetL9 and in figure 10(b) for JetL5, JetL5-75d and JetL5-60d. The algorithm does not permit to have the convection velocity close to the nozzle lips and close the flat plate.

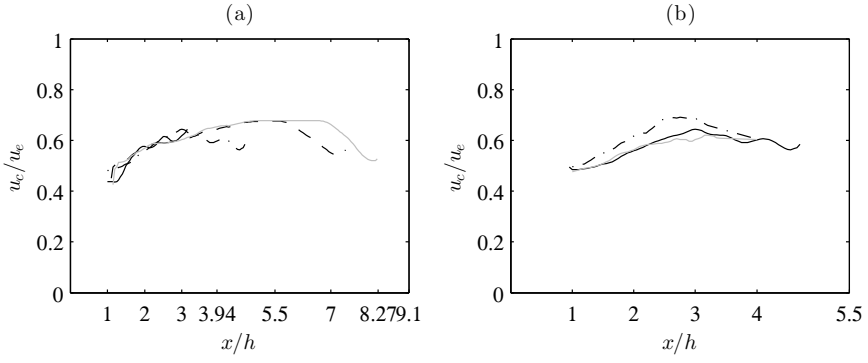

Figure 10. Convection velocity of the large-scale structures in the shear layers for (a) —— JetL3, —·— JetL5, — — — JetL8, and —— JetL9 and (b) —— JetL5, —— JetL5-75d, and —·— JetL5-60d.

In figure 10(a), for all cases, the convection velocities are of about $0.50u_e$ at $x = h$. Farther downstream, they increase slightly until it reaches the location $2h$ upstream from the flat plate. A rapid grow just before the plate is then visible. The maximal convection velocities between $x = h$ and the location $2h$ upstream from the flat plate are equal to $0.62u_e$, $0.64u_e$, $0.67u_e$ and $0.68u_e$ for JetL3, JetL5, JetL8 and JetL9, respectively. In figure 10(b), the convection velocities for JetL5 and JetL5-75d show the same variations with a maximal value of $0.64u_e$ located around $x = 3h$ whereas the convection velocity of JetL5-60d reaches a peak value of $0.69u_e$ at $x = 2.5h$. Overall, the mean convection velocity of the large-scale structures along the lipline is of about $0.60u_e$. This result is in good agreement with the theoretical value of $u_c/u_e = 0.57$ and with the experimental results of Panda *et al.*[27] who measured a convection velocity of $0.60u_e$ for an ideally expanded rectangular supersonic jet with an exit Mach number of $\mathcal{M}_e = 1.3$.

III.E. Acoustic results

Sound pressure levels (SPL) obtained for JetL3, JetL5, JetL8 and JetL9 at $x = 0$ and $y = 1.5h$ are displayed in figure 11 as a function of the Strouhal number $St_h = fh/u_e$. Several tones emerge, especially for JetL3 and JetL5 for which about ten tones are visible. A large number of tones were also observed experimentally by Norum[10] for a supersonic rectangular jet impinging on a flat plate normally. The frequency of the tones, whose level are about 5 dB higher than the broadband noise, are given in table 6.

In the sound spectrum of JetL3 shown in figure 11(a), the tone frequencies are not the harmonics of one fundamental frequency. Instead, they can be given by the linear combination of the tone frequencies at Strouhal numbers $St_1 = 0.115$ and $St_2 = 0.255$, namely $St_3 = St_1 + St_2$, $St_4 = 2St_1 + St_2$, $St_5 = St_1 + 2St_2$, $St_6 = 2St_1 + 2St_2$ and $St_7 = 3St_1 + 2St_2$. A similar result was obtained by Tam and Norum[11] on

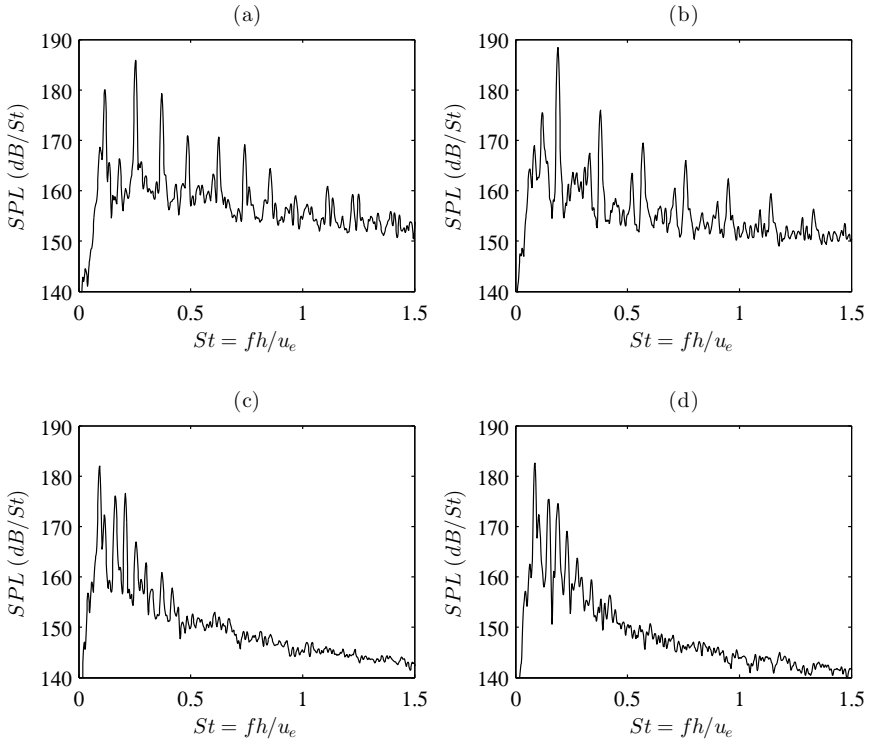

Figure 11. Sound Pressure Levels (SPL) at $x = 0$ and $y = 1.5h$ as a function of the Strouhal number for (a) JetL3, (b) JetL5, (c) JetL8 and (d) JetL9.

	St_1	St_2	St_3	S_4	St_5	St_6	St_7
JetL3	0.115	**0.255**	0.37	0.485	0.625	0.74	0.855
JetL5	0.12	**0.19**	0.33	0.38	0.52	0.57	0.76
JetL8	**0.092**	0.165	0.21	0.255	–	–	–
JetL9	**0.085**	0.145	0.19	0.23	–	–	–

Table 6. Strouhal numbers emerging in the spectra of figure 11. The Strouhal number of the main tone of each case appear in bold.

the experimental data of Norum.[10] Several tone frequencies were almost always obtained, and for some experimental conditions, two tone frequencies and their linear combinations were observed. Moreover, as detailed earlier, the jets parameters are similar to those of the experimental study of Thurow et al.[13] and they found for $L = 3.94$ the seven tone frequencies observed in the present study. Eight other tone frequencies were also obtained by Thurow et al.[13] and can be due to the rectangular nozzle in the experiment compared to the ideal planar present jets. For JetL5 in figure 11(b), a fundamental tone frequency at $St = 0.19$ and its first six harmonics can be seen. Two other tone frequencies $St_1 = 0.12$ and $St_3 = 0.33$ are visible and $St_5 = St_2 + St_3$. The agreement is excellent with the experimental data of Thurow *et al.*[13] who obtained a fundamental tone frequency occurring at $St_{exp} = 0.20$. For JetL8 and JetL9 in figures 11(c) and 11(d), four tone frequencies are visible and only the third one St_3 is observed experimentally by Thurow *et al.*[13] in each case. However, for nozzle distances of $8.27h$ and $9.1h$, the experimental jet of Thurow can not be seen as planar any more and differences are expected. It can also be noted that in the two latter cases, $St_4 = St_1 + St_2$. Finally, the case JetL5 is the most resonant of our four cases where the angle of impact is $\theta = 90$ degrees with a maximum sound pressure level of 188 dB/St. It was also the most resonant case in the experiment of Thurow *et al.*[13]

Sound pressure levels acquired for JetL5, JetL5-75d and JetL5-60d at $x = 0$ and $y = 1.5h$ are shown in figure 12. As earlier, several tone frequencies are noted and those whose levels are about 5 dB higher than the broadband noise are given in table 7. For JetL5-75d, in figure 7(b), two emerging tone frequencies are visible at $St_1 = 0.19$ and $St_2 = 0.25$. The first one is the same one as for the case JetL5 in figure 12(a)

and the latter one do not exist in JetL5. For JetL5-60d, in figure 12(c), there is no clear tone frequency. However, the maximum sound pressure level seems to be found around $St = 0.25$.

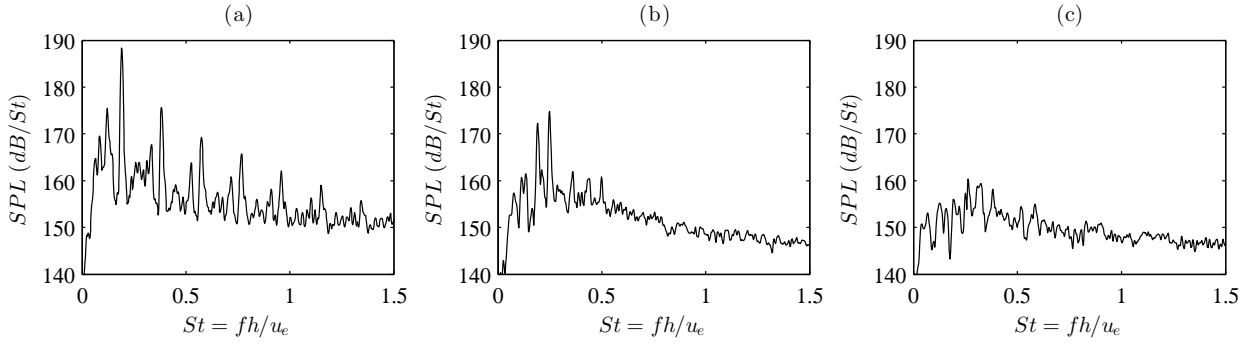

Figure 12. Sound Pressure Levels (SPL) at $x = 0$ and $y = 1.5h$ as a function of the Strouhal number for (a) JetL5, (b) JetL5-75d and (c) JetL5-60d.

	St_1	St_2	St_3	S_4	St_5	St_6	St_7
JetL5	0.12	**0.19**	0.33	0.38	0.52	0.57	0.76
JetL5-75d	0.19	**0.25**	–	–	–	–	–
JetL5-60d	0.25	–	–	–	–	–	–

Table 7. Strouhal numbers emerging in spectra of figure 12. The Strouhal number of the main tone of each case appear in bold. The Strouhal number of the maximum sound pressure level for JetL5-60d appears in grey.

III.F. Skewness and kurtosis factors

In order to investigate the non-linearity of the acoustic waves generated by the impingement, the properties of the pressure has been examined at $x = 0$ and $y = 8.5h$. Figure 13(a) displays the fluctuating pressure at this point for JetL5. Weak shock waves and N-shaped waves with sharp compressions associated with gradual expansions are visible. These shapes are similar to those obtained by de Cacqueray and Bogey[28] in the acoustic field of an overexpanded jet[24] at $\mathcal{M}_j = 3.3$. Moreover, for some times, the amplitude exceeds $0.15P_{amb}$. This is the case around $t = 250h/u_e$. A zoom centered around this time is presented in figure13(b). Two strong shock waves are found at $t_1 = 242h/u_e$ and $t_2 = 253h/u_e$. In order to quantify this observation, figure 13(c) shows the probability density function (PDF) of the fluctuating pressure normalized by the standard deviation as well as the skewness and kurtosis factors. A skewness factor of $S = 0.59$ and a kurtosis factor of $K = 3.99$ are obtained, indicating a strong non-linearity and intermittency in the signal, respectively. This behaviour with strong intermittent shock waves seems to correspond to that of the crackle noise first defined by Ffowcs-Williams *et al.*,[29] who obtained this specific noise when the skewness factor exceeds 0.4. Moreover, the evolution visible in figure 13(b) agrees well with the results of Baars and Tinney.[30] In an experimental Mach 3 jet, they found out that strong shock waves, responsible for the crackle noise, are often present in groups of multiple shocks.

	JetL3	JetL5	JetL8	JetL9	JetL5-75d	JetL5-60d
$SPL_{max}(dB/S_t)$	185	188	182	183	175	160
Skewness	0.39	0.59	0.27	0.29	0.25	0.21
Kurtosis	3.16	3.99	3.36	3.25	3.17	3.42

Table 8. Maxima levels in the sound spectra of figures 11 and 12, skewness and kurtosis factors of the fluctuating pressure at $x = 0$ and $y = 8.5h$.

For the six jets studied, the maxima of sound pressure levels shown in figures 11 and 12, and the skewness and the kurtosis factors at $x = 0$ and $y = 8.5h$, are reported in table 8. A significant correlation appears between the maxima in the sound spectra of figures 11 and 12, and the skewness factors of the fluctuating pressure at $x = 0$ and $y = 8.5h$. Moreover, the most resonant case, JetL5, show the strongest intermittency of the fluctuating pressure with a kurtosis factor of 3.99.

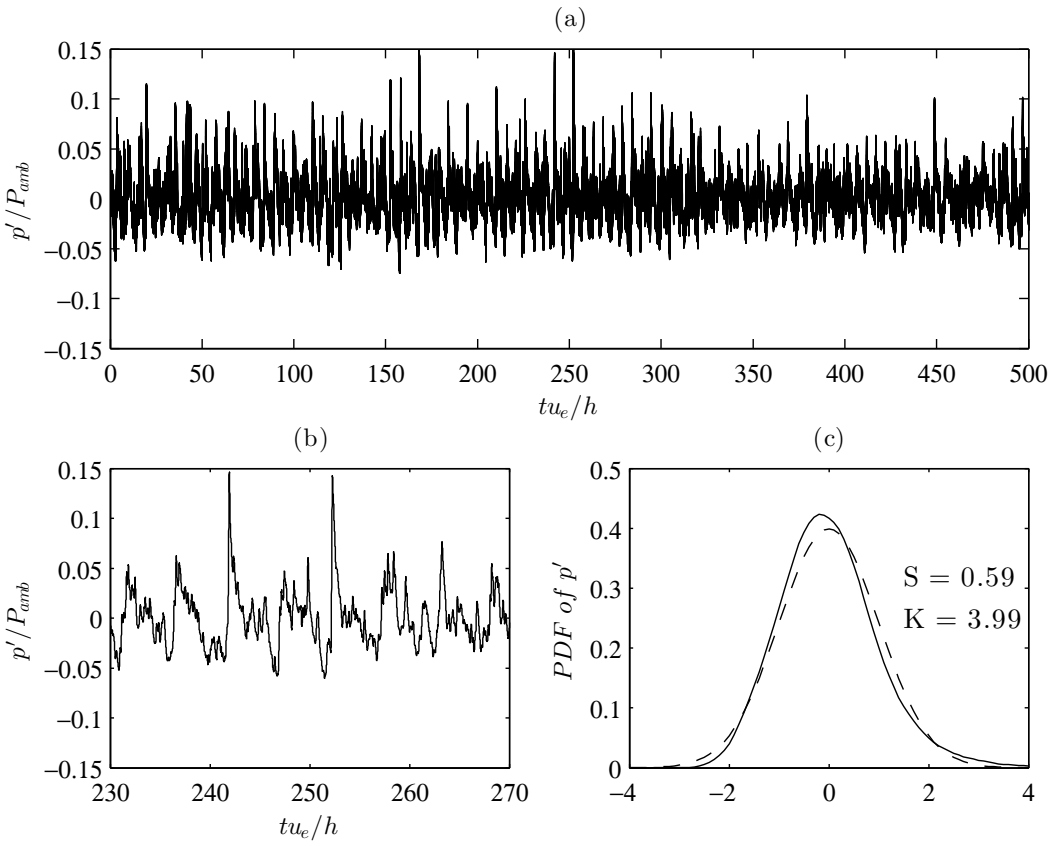

Figure 13. Fluctuating pressure at $x = 0$ and $y = 8.5h$ for JetL5: (a) time variations over the entire simulation, (b) variations over a short period and (c) —— probability density function (— — — probability density function of a Gaussian distribution).

IV. Aeroacoustic feedback mechanism

IV.A. Tone frequencies

In order to explain the tone frequencies found experimentally, Powell[1] was the first to suggest that a feedback mechanism establishes between the nozzle lips and the flat plate. This mechanism consists of two steps. First, in the shear layer, a coherent structure is convected downstream from the nozzle to the plate. The structure impinges on the plate, and generates an acoustic wave propagating upstream towards the nozzle. This wave is then reflected by the nozzle lip, excites the shear layer, and leads to the formation of a new coherent structure. The fundamental period T_0 of this feedback loop corresponds to the sum of the time necessary for a coherent structure to travel downstream from the nozzle to the plate and the time of propagation of an acoustic wave from the plate to the nozzle, yielding

$$T_0 = \int_0^L \frac{1}{u_c(x)} dx + \frac{L}{c_0} = \frac{N+p}{f} \tag{3}$$

where $u_c(x)$ is the local convection velocity of the large-scale structures in the shear layers, c_0 is the speed of sound outside of the jet, p is a phase lag at the nozzle exit, and the mode number N indicates the number of time the feedback mechanism occurs during the fundamental period T_0.

Powell[1] argued that the phase lag p is not necessarily null because the reflection of the acoustic wave on the nozzle lips and the creation of a coherent structure are not simultaneous phenomena. In experiments, Krothapalli *et al.*[5] found for instance $p = 0$ for subsonic round jets and $p = -0.4$ for supersonic round jets. Later, Ho and Nosseir[2] and Nosseir and Ho[3] investigated the near field pressure of jets impinging on a flat plate normally, and proposed an empirical model in order to predict the frequencies of the feedback mechanism, this model writes

$$\frac{N}{f} = \frac{L}{u_c} + \frac{L}{c_0} \tag{4}$$

where u_c is the mean convective velocity of the large-scale structures in the shear layers. Here, the phase lag p is considered null.

The Strouhal number of the tone frequencies obtained for the present jets in figures 11 and 12 are shown in figure 14 as a function of the nozzle-to-plate distance L/h. Only the fundamental tone frequencies, which are not harmonics of other tone frequencies and which are called source tone frequencies in the following, are represented. The tone frequencies observed in the experiments of Thurow *et al.*,[13] as well as the tone frequencies predicted by relation (4) with a mean value of convective velocity $u_c = 0.60u_e$, are also plotted. As mentioned previously, a good agreement is found between the simulation and the experimental data. Moreover, the tone frequencies seem to be well predicted by the empirical model.

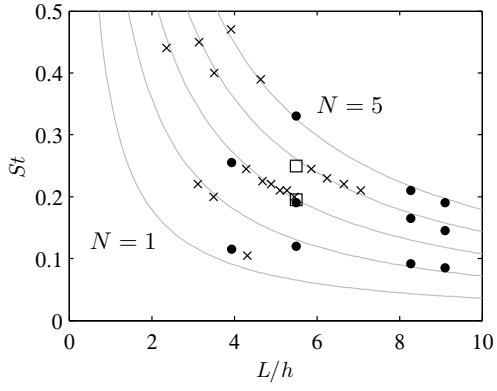

Figure 14. Strouhal number of the tone frequencies obtained: • for JetL3, JetL5, JetL8 and JetL9, □ for JetL5-75d, and × experimentally by Thurow *et al.*[13] The grey lines show the values predicted by the model (4) using $u_c = 0.60u_e$.

For JetL3, with $L/h = 3.94$, the two source tone frequencies, at $St_1 = 0.115$ and $St_2 = 0.255$, correspond to the first mode and the third mode predicted by the model. For JetL5, with $L/h = 5.5$, the three source tone frequencies, at $St_1 = 0.12$, $St_2 = 0.19$ and $St_3 = 0.33$, can be associated with the second mode, the third mode and the fifth mode. For JetL8 and JetL9, with $L/h = 8.27$ and $L/h = 9.1$, the three source tone frequencies can be connected with the second mode, the fourth mode and the fifth mode.

The influence of the angle of impact can be explored by comparing JetL5, JetL5-75d and JetL5-60d. For JetL5, the dominant source tone $St_2 = 0.19$ is linked to the third mode of the model (4). For JetL5-75d, the two observale tones, at $St_1 = 0.19$ and $St_2 = 0.25$, correspond to the third and the fourth modes of the model. Finally, for JetL5-60d, no tones are represented in the figure 14, because they are not clearly visible in the spectra. The maximum sound pressure level is however reached around $St = 0.25$. Thus, when the angle of impact deviates from 90 degrees, there seems to be an evolution from the third mode to the fourth mode predicted by (4). A similar jump is observed in figure 14 when the nozzle-to-plate distance increases from $5.5h$ to $5.8h$ in the experiment of Thurow *et al.*[13]

IV.B. Fourier decomposition of the pressure field

For each jet, the pressure field in the (x, y) plane has been recorded every 50^{th} time steps. The results are arranged in a $M \times N$ matrix P_{all}:

$$P_{all} = \begin{bmatrix} P_1^1 & P_1^2 & . & P_1^N \\ P_2^1 & P_2^2 & . & P_2^N \\ . & . & . & . \\ P_M^1 & P_M^2 & . & P_M^N \end{bmatrix} \tag{5}$$

where N is the number of samplings, and $M = n_x \times n_y$ is the total number of points. The pressure field obtained at a given time is thus provided by one column of P_{all}. A Fast Fourier Transform is applied to each row of the matrix P_{all}. In this way, for a given frequency, amplitude and phase fields can be displayed.

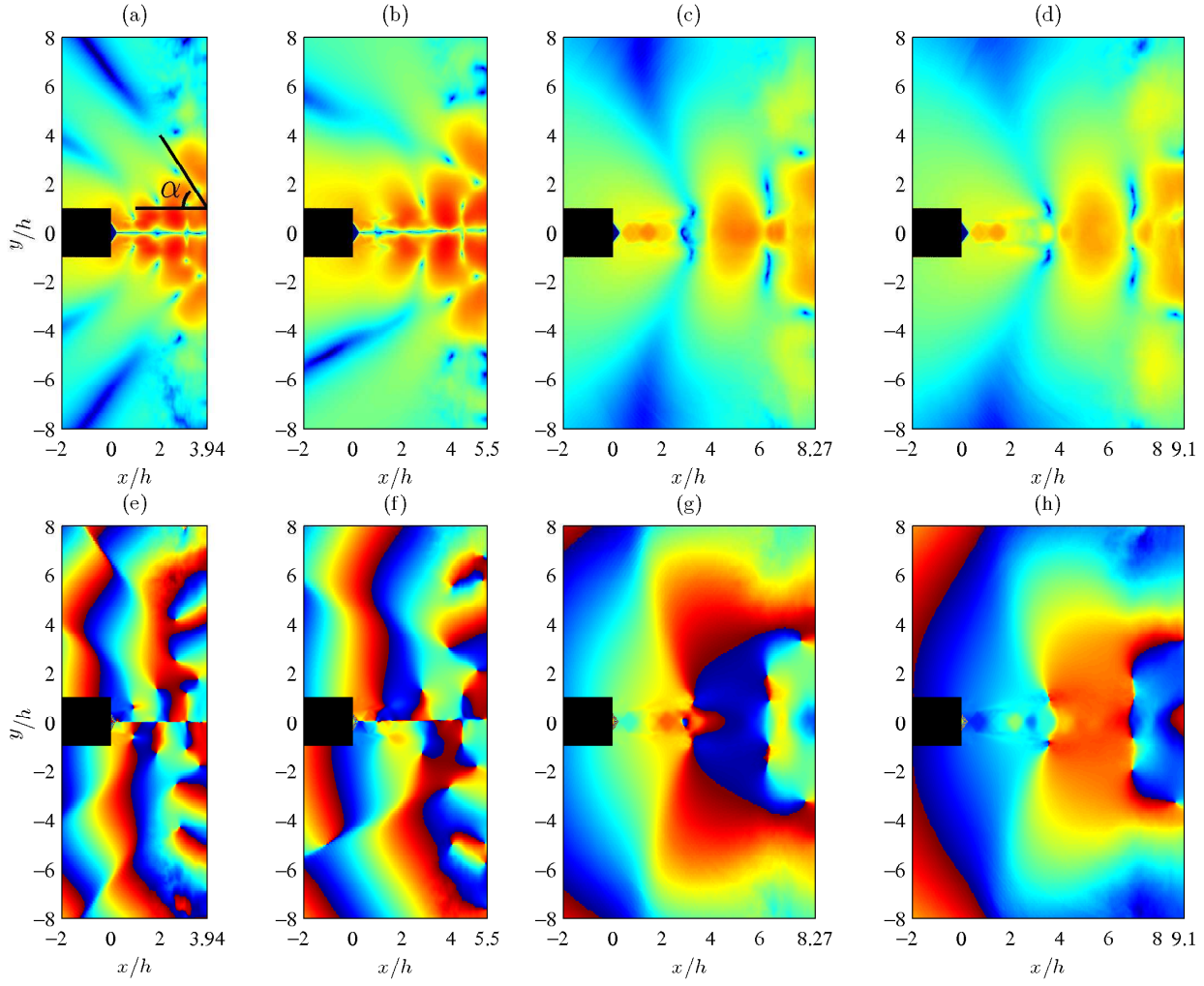

Figure 15. Amplitude (top) and phase (bottom) fields obtained for the dominant tone frequency in (a) and (e) JetL3 ($St_h = 0.255$), (b) and (f) JetL5 ($St_h = 0.19$), (c) and (g) JetL8 ($St_h = 0.092$) and (d) and (h) JetL9 ($St_h = 0.085$).

For the four jets with $\theta = 90$ degrees, the dominant tone frequencies are considered. The amplitude fields are shown in the top views of figure 15, and the phase fields are displayed in the bottom views. The latter fields enable to identify the nature of the modes. The dominant source tone frequencies in JetL3 and JetL5 correspond to antisymmetric modes because there is a 180 degree phase shift visible with respect to the jet axis in figures 15(e) and 15(f). On the contrary, the dominant source tone frequencies in JetL8 and JetL9 are associated with a symmetric mode, as the phase shift is null with respect to the jet axis in figures 15(g) and 15(h). For planar high subsonic jets impinging on a flat plate, Arthurs and Ziada[9] also found that the source tone frequencies obtained in the spectra are generated by both symmetric and antisymmetric modes.

Besides, these results agree well with the theoretical developments of Tam and Norum[11] who proposed that the upstream propagating waves of the feedback mechanism are due to neutral acoustic wave modes of the jet. Such modes are characterized by a wave number k and an angular frequency ω both real. For a supersonic jet, the existence of acoustic modes propagating upstream was demonstrated by Tam et Hu.[31] Such waves propagate upstream along the shear layer of the jet. Tam and Norum[11] used a vortex sheet jet model to predict these modes and found an allowable frequency range for each upstream propagating neutral acoustic wave mode of the jet flow. The two dominant tone frequencies of JetL3 and JetL5, which are associated to symmetric modes, fall into the first symmetric allowable band given by this model. Moreover, the two dominant tone frequencies of JetL8 and JetL9, linked to antisymmetric modes, take place into the first antisymmetric allowable band given by this model. The experimental results of Norum[10] were also in

agreement with this model.

The amplitude fields of the dominant tone frequencies for JetL3, JetL5, JetL8 and JetL9, represented in the top of figure 15, all exhibit a cell structure between the nozzle lips and the flat plate. By considering the two semi-cells near the nozzle lips and the plate as one cell, the cell structure contain three cells for JetL3 and JetL5 in figures 15(a) and 15(b) and two cells for JetL8 and JetL9 in figures 15(c) and 15(d). Thus, the number of cells correspond to the mode number predicted by the model of Ho and Nosseir.[2] Indeed, the third mode was identified for the dominant source tone frequencies of the two first jets, and the second mode for the two others. Moreover, for the present jets, the amplitude fields of all tone frequencies have been examined and the number of visible cells corresponds in all cases to the mode number given by the model of Ho and Nosseir.[2]

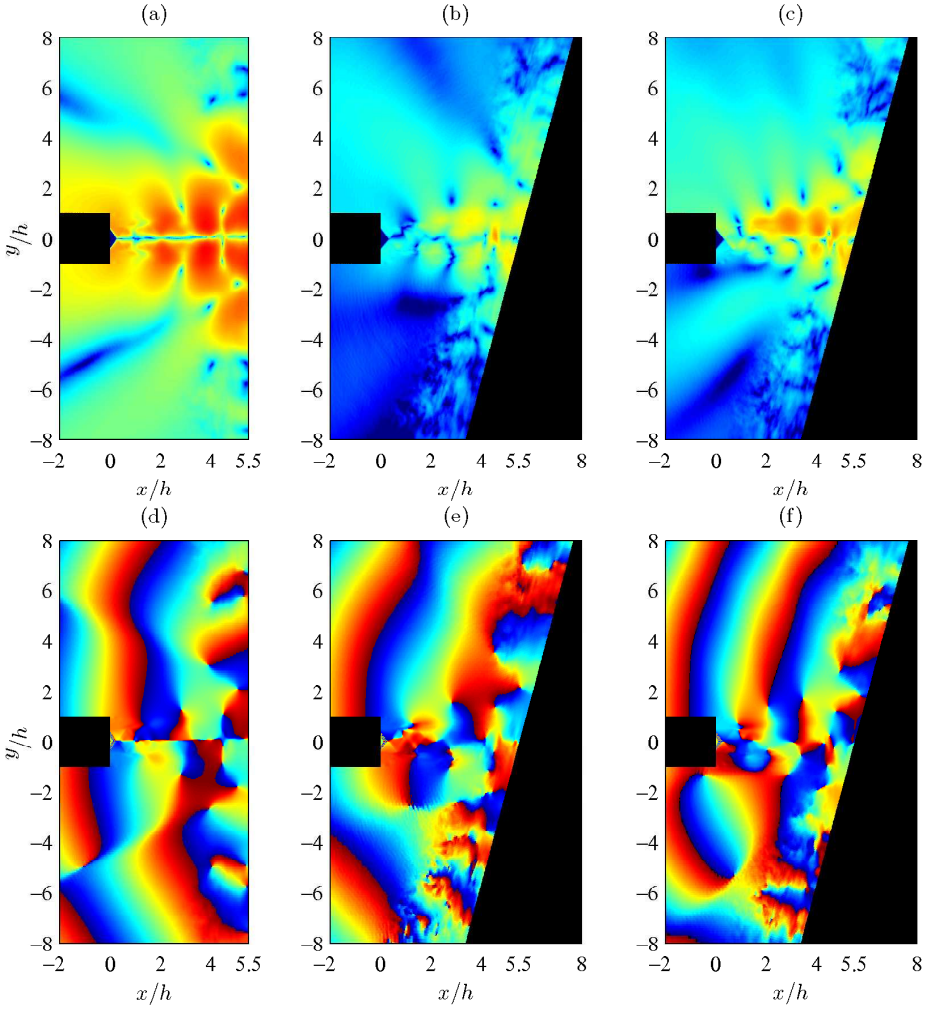

Figure 16. Amplitude (top) and phase (bottom) obtained for the pressure fields for (a) and (d) JetL5 at $St_h = 0.19$, JetL5-75d (b) and (e) at $St_h = 0.19$ and (c) and (f) at $St_h = 0.25$.

Information on the sound sources are also provided by the amplitude an phase fields of figure 15. For a better description of these fields, let α be the angle at the impingement region between the upstream direction and the waves propagating from the flat plate, illustrated in figure 15(a).

For the dominant tone frequency of JetL3, in figures 15(a) and 15(e), three acoustic contributions can be seen by analysing the intense spots and the destructive interferences in the amplitude field and by looking at the phase contours in the phase field. Indeed, the phase contours in the near acoustic field appear to spread concentrically from three regions. The first visible acoustic contribution can be seen in the shear layers of the jet and in the near field on each side of the nozzle, for $0 < \alpha < 30$ degrees and correspond to the upstream propagating neutral acoustic wave mode of the jet. The second contribution is visible for $30 < \alpha < 50$ degrees in figure 15(e) as the phase contours in this region seem to spread from a point around $x = 2.5h$

and $y = 1.5h$. This position coincides with an intense spot in the magnitude field in figure 15(a). Finally, the third acoustic contribution is visible for $\alpha > 50$ degrees in figure 15(e) and seems to propagate from a point on the plate at $y = 3h$. Again, this position matches an intense spot in the magnitude field displayed in figure 15(a). Finally, destructive interferences can be seen for $\alpha = 30$ and $\alpha = 50$ degrees between the three acoustic contributions in figure 15(e) with a strong reduction of the amplitude in these directions. The same reasoning can be applied to the dominant source tone frequency of JetL5, in figures 15(b) and 15(f). In this way, two acoustic contributions can be observed. The first one is still due to the upstream propagating neutral acoustic wave mode of the jet and can be seen for $0 < \alpha < 30$ degrees and the second one seems to originate from a point located on the plate at $y = 3.5h$. Destructive interferences can also be seen between the two acoustic contributions for $\alpha = 40$ degrees. For the dominant tone frequencies of JetL8 and JetL9, two acoustic contributions seem to emerge. One still due to the upstream propagating neutral acoustic wave mode of the jet and another propagating from a point located close to the plate. However, the large wavelengths of these modes compared to the computational domain makes it difficult to look at the phase contours or to see destructive interferences.

The amplitude and phase fields obtained for the dominant source tone frequency of JetL5 and the two tone frequencies of JetL5-75d are displayed in figure 16. For JetL5-75d, the amplitude fields in figures 16(b) and 16(c) exhibit a cell structure, as in figure 16(a) for the dominant tone frequency of JetL5. There are three and four cells visible in figures 16(b) and 16(c), respectively, corresponding to the third and the fourth modes of the model of Ho and Nosseir.[2] This support the hypothesis of a switch from the third mode to the fourth mode, mentioned previously, as the angle of impact deviates from 90 degrees.

IV.C. Hydrodynamic-acoustic standing wave

The cell structures noted in the amplitude fields of figures 15 and 16 may be due to the presence of an hydrodynamic-acoustic standing wave. Indeed, when a feedback mechanism establishes in a flow, such waves can be obtained. In the experiment of Panda *et al.*[27] on a screeched supersonic jet, an hydrodynamic-acoustic standing wave was for instance observed, corresponding to the sum of hydrodynamic coherent structures in the shear layers propagating downstream and acoustic waves propagating upstream.

A simple model can be built to determine the wave number of the hydrodynamic-acoustic standing waves in the present jets. Let ω be the angular frequency of the feedback mechanism and k_p et k_a the wave numbers of the hydrodynamic coherent structures and of the acoustic waves, respectively. In the shear layer, the resulting fluctuating pressure can be written as

$$p'(x,t) = A_a sin(k_a x + \omega t + \phi_a) + A_p sin(k_p x - \omega t + \phi_p) \tag{6}$$

where A_a, A_p, ϕ_a and ϕ_p are the amplitudes and phase shifts of the acoustic waves and of the hydrodynamic structures. Then, the quadratic mean value of the fluctuating pressure is

$$p'_{rms}(x) = \frac{1}{T}\int_0^T p'(x,t)^2 dt = \frac{A_a^2}{2} + \frac{A_p^2}{2} - A_a A_p cos\left((k_a + k_p)x + \phi_a + \phi_p\right) \tag{7}$$

where $T = 2\pi/\omega$ is the time period. The wave number k_{sw} of the hydrodynamic-acoustic standing wave is thus equal to $k_p + k_a$. By noting that $L_{sw} = 2\pi/k_{sw}$ is the wavelength of the hydrodynamic-acoustic standing wave, and that $k_p = \omega/u_c$ and $k_a = \omega/c_0$, one obtains

$$\frac{1}{L_{sw}} = \frac{f}{c_0} + \frac{f}{u_c} \tag{8}$$

where $f = 2\pi/\omega$, c_0 is the speed of sound outside of the jet and u_c is the mean convective velocity of large-scale structures in the shear layers.

As seen in figures 15 and 16, there is a whole number N of cells between the nozzle lips and the flat plate. Considering that the cell structure obtained in the amplitude fields in figures 15 and 16 corresponds to an hydrodynamic-acoustic standing wave, the nozzle-to-plate distance L is a multiple of the wavelength, yielding $L_{sw} = L/N$. Then, the relation (8) becomes

$$\frac{N}{f} = \frac{L}{c_0} + \frac{L}{u_c} \tag{9}$$

The relation (9) is identical to the relation (4) given by the model of Ho and Nosseir,[2] indicating that the number of cells of the standing wave is also the mode number. Thus the aeroacoustic feedback mechanism occurring between the nozzle lips and the flat plate corresponds to the formation of an hydrodynamic-acoustic standing wave as defined by Panda *et al.*[27]

V. Conclusion

In this paper, the hydrodynamic and acoustic properties of six planar supersonic jets computed by compressible large-eddy simulations (LES) using low-dissipation schemes are presented. The jets are ideally expanded, and have a Mach number of $\mathcal{M}_e = 1.28$, and a Reynolds number of $Re_h = 5 \times 10^4$. Four jets impinging on a flat plate normally, and two other impinging jets with angles of impact of $\theta = 60$ and $\theta = 75$ degrees are considered. Mean velocity flows and snapshots of density, fluctuating pressure and vorticity are described. The results agree well with experimental data. The development of the shear layers is investigated by computing rms values of velocity fluctuations and convective velocities of large-scale structures. The mean convective velocities are in line with the theoretical model proposed by Papamoschou and Roshko[26] and with the experimental values found by Panda *et al.*[27]

The near pressure fields are then detailed. First, sound pressure levels are computed. They revealed several tones emerging, which agree well with the measurements of Thurow *et al.*,[13] as well as with the empirical model of Ho and Nosseir.[2] Finally, the skewness and kurtosis factors of the fluctuating pressure are computed, and properties typical of crackle noise are observed for the most resonant case. A Fourier decomposition is also applied to the near pressure fields in the (x, y) plane. The amplitude and the phase fields of the dominant source tone frequencies for each case are considered. For the cases of normal impact, the antisymmetric or symmetric natures of the modes are identified. The results are in agreement with the theoretical developments of Tam and Norum.[11] Besides, an hydrodynamic-acoustic standing wave is found for each source tone frequency, as observed by Panda *et al.*[27] on a screeched supersonic jet. The number of cells in the structure corresponds to the mode number of the model given by Ho and Nosseir.[2] As the angle of impact deviates from 90 degrees, a jump from one mode to a higher mode and a reduction of the intensity of the feedback mechanism are observed.

In further work, the underlying physics of the feedback mechanism will be explored. This will be done by extracting the most energetic modes by proper orthogonal decomposition and by using dynamic mode decomposition. Moreover, the theoretical developments of Tam and Norum[11] will be applied to the present jets.

Acknowledgments

This work was performed using HPC resources of P2CHPD (Pôle de Calcul Hautes Performances Dédiés) and IDRIS (Institut du Développement et des Ressources en Informatique Scientifique) under the allocation 2014-2a0204 made by GENCI (Grand Equipement National de Calcul Intensif). This work was performed within the framework of the Labex CeLyA of Université de Lyon, within the program "Investissements d'Avenir" (ANR-10-LABX-0060/ ANR-11-IDEX-0007) operated by the French National Research Agency (ANR).

References

[1]Powell, A., "On edge tones and associated phenomena", *Acta Acust. United Ac.*, Vol. 3, 1953, pp. 233-243.

[2]Ho, C.M. and Nosseir, N.S., "Dynamics of an impinging jet. Part 1. The feedback phenomenon", *J. Fluid Mech.*, Vol. 105, 1981, pp. 119-142.

[3]Nosseir, N.S. and Ho, C.M., "Dynamics of an impinging jet. Part 2. The noise generation", *J. Fluid Mech.*, Vol. 116, 1982, pp. 379-391.

[4]Henderson, B. and Powell, A., "Experiments concerning tones produced by an axisymmetric choked jet impinging on flat plates", *J. Sound Vib.*, Vol. 168, No. 2, 1993, pp. 307-326.

[5]Krothapalli, A., Rajkuperan, E., Alvi, F. and Lourenco, L., "Flow field and noise characteristics of a supersonic impinging jet", *J. Fluid Mech.*, Vol. 392, 1999, pp. 155-181.

[6]Henderson, B., Bridges, J. and Wernet, M., "An experimental study of the oscillatory flow structure of tone-producing supersonic impinging jets", *J. Fluid Mech.*, Vol. 542, 2005, pp. 115-126.

[7]Risborg, A. and Soria, J., "High-speed optical measurements of an underexpanded supersonic jet impinging on an inclined plate", *28th International Congress on High-Speed Imaging and Photonics*, Vol. 7126, 2009.

[8]Buchmann, N.A., Mitchell, D.M., Ingvorsen, K.M., Honnery, D.R., and Soria, J., "High spatial resolution imaging of a supersonic underexpanded jet impinging on a flat plate", *Sixth Australian Conference on Laser Diagnostics in Fluid Mechanics and Combustion*, Vol. 116, 2011

[9]Arthurs, D. and Ziada, S., "Self-excited oscillations of a high-speed impinging planar jet", *J. Fluids Struct.*, Vol. 34, 2012, pp. 236-258.

[10]Norum, T.D., "Supersonic rectangular jet impingement noise experiments", *AIAA J.*, Vol. 29, 1991, pp. 1051-1063.

[11]Tam, C.K.W. and Norum, T.D., "Impingement tones of large aspect ratio supersonic rectangular jets", *AIAA J.*, Vol. 30, 1992, pp. 304-311.

[12]Hourigan, K., Rudman, M. and Brocher, E., "The feedback loop in impinging two-dimensional high-subsonic and supersonic jets", *Experimental Thermal and Fluid Science*, Vol. 12, 1996, pp. 265-270.

[13]Thurow, B., Samimy, M. and Lempert, W., "Structure of a supersonic impinging rectangular jet via real-time optical diagnostics", *32nd AIAA Fluid Dynamics Conference*, 2002

[14]Nonomura, T., Tsutsumi, S., Takaki, R., Shima, E. and Fujii, K., "Impact of Spatial and Temporal Resolution on the Aeroacoustic Wave from a Two-dimensional Impinging Jet", *7th International Conference on Computational Fluid Dynamics*, 2012, ICCFD7-3103.

[15]Nonomura, T., Goto, Y. and Fujii, K., "Aeroacoustic waves generated from a supersonic jet impinging on an inclined flat plate", *Int. J. Aeroacoust.*, Vol. 10, 2011, pp. 401-426.

[16]Tsutsumi, S., Nonomura, T., Fujii, K., Nakanishi, Y., Okamoto, K. and Teramoto, S., "Analysis of Acoustic Wave from Supersonic Jets Impinging to an Inclined Flat Plate", *7th International Conference on Computational Fluid Dynamics*, 2012, ICCFD7-3104.

[17]Dargaud, J.B., Troyes, J., Lamet, J.M., Tessé, L., Vuillot, F. and Bailly, C., "Numerical Study of Solid-Rocket Motor Ignition Overpressure Wave Including Infrared Radiation", *J. Prop. and Power*, Vol. 30, No. 1, 2014, pp. 164-174.

[18]Bogey, C. and Bailly, C., "A family of low dispersive and low dissipative explicit schemes for flow and noise computations", *J. Comput. Phys.*, Vol. 194, No. 1, 2004, pp. 194-214.

[19]Berland, J., Bogey, C., Marsden, O. and Bailly, C., "High-order, low dispersive and low dissipative explicit schemes for multiple-scale and boundary problems", *J. Comput. Phys.*, Vol. 224, No. 2, 2007, pp. 637-662.

[20]Tam, C.K.W. and Dong, Z., "Wall boundary conditions for high-order finite-difference schemes in computational aeroacoustics", *Theor. Comput. Fluid Dyn*, Vol. 6, 1994, pp. 303-322

[21]Bogey, C. and Bailly, C., "Large eddy simulations of transitional round jets: influence of the Reynolds number on flow development and energy dissipation", *Phys. Fluids*, Vol. 18, No. 065101, 2006, pp. 1-14.

[22]Bogey, C. and Bailly, C., "Turbulence and energy budget in a self-preserving round jet: direct evaluation using large eddy simulation", *J. Fluid Mech.*, Vol. 627, 2009, pp. 129-160.

[23]Bogey, C., de Cacqueray, N. and Bailly, C., "A shock-capturing methodology based on adaptative spatial filtering for high-order non-linear computations", *J. Comput. Phys.*, Vol. 228, 2009, pp. 1447-1465.

[24]de Cacqueray, N. and Bogey, C. and Bailly, C., "Investigation of a High-Mach-Number Overexpanded Jet Using Large-Eddy Simulation", *AIAA J.*, Vol. 49, No. 10, 2011, pp.2171-2182.

[25]Bogey, C., Marsden, O. and Bailly, C., "Large-eddy simulation of the flow and acoustic fields of a Reynolds number 10^5 subsonic jet with tripped exit boundary layers", *Phys. Fluids*, Vol. 23, 2011, pp. 035104.

[26]Papamoschou, D. and Roshko, A., "The compressible turbulent shear layer: an experimental study", *J. Fluid Mech.*, Vol. 197, 1988, pp. 453-477.

[27]Panda, J., Raman, G. and Zaman, K.B.M.Q., "Underexpanded screeching jets from circular, rectangular and elliptic nozzles", *3th AIAA/CEAS Aeroacoustics conference*, 1997, AIAA Paper 97-1623

[28]de Cacqueray, N. and Bogey, C., "Noise of an overexpanded Mach 3.3 jet: non-linear propagation effects and correlations with flow", *Int. J. Aeroacoust.*, Vol. 13, No. 7, 2014, pp. 607-632.

[29]Ffowcs-Williams, J.E., Simson, J. and Virchis, V.J., "Crackle: An annoying component of jet noise", *J. Fluid Mech.*, Vol. 71, 1975, pp. 251-271.

[30]Baars, W. J. and Tinney, C. E., "Quantifying crackle-inducing acoustic shock-structures emitted by a fully-expanded Mach 3 jet", *19th AIAA/CEAS Aeroacoustics conference*, 2013, AIAA Paper 2013-2081

[31]Tam, C.K.W. and Hu, F.Q., "On the three families of instability waves of high-speed jets", *J. Fluid Mech.*, Vol. 201, 1989, pp. 447-483.